



HAL
open science

Determination of Microporous and Mesoporous Surface Areas and Volumes of Mesoporous Zeolites by Corrected t -Plot Analysis

Lucie Desmurs, Anne Galarneau, Claudia Cammarano, Vasile Hulea, Cyril Vaultot, Habiba Nouali, Benedicte Lebeau, T. Jean Daou, Carla Vieira Soares, Guillaume Maurin, et al.

► To cite this version:

Lucie Desmurs, Anne Galarneau, Claudia Cammarano, Vasile Hulea, Cyril Vaultot, et al.. Determination of Microporous and Mesoporous Surface Areas and Volumes of Mesoporous Zeolites by Corrected t -Plot Analysis. *ChemNanoMat*, 2022, 8 (4), pp.e202200051. 10.1002/cnma.202200051. hal-03647181

HAL Id: hal-03647181

<https://hal.science/hal-03647181>

Submitted on 20 Apr 2022

HAL is a multi-disciplinary open access archive for the deposit and dissemination of scientific research documents, whether they are published or not. The documents may come from teaching and research institutions in France or abroad, or from public or private research centers.

L'archive ouverte pluridisciplinaire **HAL**, est destinée au dépôt et à la diffusion de documents scientifiques de niveau recherche, publiés ou non, émanant des établissements d'enseignement et de recherche français ou étrangers, des laboratoires publics ou privés.

Determination of Microporous and Mesoporous Surface Areas and Volumes of Mesoporous Zeolites by Corrected *t*-plot Analysis

Lucie Desmurs,^a Anne Galarneau,^{a*} Claudia Cammarano,^a Vasile Hulea,^a Cyril Vaultot,^{b,c} Habiba Nouali,^{b,c} Benedicte Lebeau,^{b,c} T. Jean Daou,^{b,c} Carla Vieira Soares,^a Guillaume Maurin,^a Maciej Haranczyk,^d Isabelle Batonneau-Gener,^e Alexander Sachse^e

^a Institut Charles Gerhardt Montpellier, ICGM, Univ Montpellier, CNRS, ENSCM, Montpellier, France.

^b Université de Haute Alsace (UHA), CNRS, IS2M UMR 7361, F-68100, Mulhouse, France.

^c Université de Strasbourg, F-67000 Strasbourg, France.

^d IMDEA Materials Institute, C/Eric Kandel 2, 28906 - Getafe, Madrid, Spain.

^e Institut de Chimie des Milieux et Matériaux de Poitiers (IC2MP), Université de Poitiers – UMR 7285 CNRS, UFR SFA, Bat. B27, 4 rue Michel Brunet, TSA 51106, 86073 Poitiers, Cedex 9, France.

ABSTRACT: Zeolites are well-known microporous catalysts, involved in many industrial applications. Their microporosity yet impedes diffusion of bulky molecules/feedstocks. To overcome this drawback, zeolites with bimodal porosity, e.g. micropores and mesopores were developed during the last decades. In this context, it is important to develop/use methods able to evaluate accurately the textural properties of micro-/mesoporous zeolites. *t*-Plot is commonly used for determining the micro- and mesopore surface areas and pore volumes. However, previously we showed that the classical *t*-plot analysis overestimates the mesopore surface areas and underestimates the micropore volumes for FAU-Y micro-/mesoporous zeolite. Measurements performed with mechanical mixtures of FAU-Y and MCM-41 allowed us to provide corrections to the *t*-plot analysis. These corrections were up to date limited to FAU structured zeolites. In the present work, we present specific corrections of the *t*-plot for a broader series of zeolites including MFI, *BEA and MOR, based on a set of mechanical mixtures of zeolites and MCM-41. Minor correction factors were required for MOR, whilst for MFI and *BEA similar corrections as for the FAU-Y were inferred for the micropore volume. As far as the surface area is concerned higher correction factors were required for MFI compared to *BEA. This corrected *t*-plot analysis was applied to characterize a great variety of mesoporous zeolites prepared by micelle-templating following a two-steps procedure.

Keywords: Hierarchical; Zeolite; micropore; mesopore; volume; surface; area; BET; nitrogen; adsorption

INTRODUCTION

Zeolites dominate the world catalyst global market due to their enormous use in oil refining and petrochemistry with growing applications in fine chemicals synthesis and environmental catalysis. Fluid catalytic cracking (FCC) and hydrocracking are the most important catalytic processes involving zeolites and in particular USY (i.e. ultra stable Y zeolite featuring FAU topology). MFI-type zeolites are used in at least 30 different industrial processes, mainly based on alkylation and isomerization reactions.¹ It is also used in FCC formulation to adjust propylene yields.¹ The conversion of bulky oil feedstocks or of biomass derivatives (sugar, lipids and lignocellulose) are widely investigated during the last years, particularly over zeolites with multimodal porosity.² These materials, containing both micropores and mesopores, are referred as hierarchical zeolites or mesoporous zeolites.²

A large variety of mesoporous zeolites^{2,3} has been reported and they can be classified as follows: (i) zeolite crystals coated by a thin layer of mesoporous material,^{3,4} (ii) micro-/mesoporous nanocomposites with large domains of both micro- and mesoporous materials,^{3,5} (iii) mesoporous materials containing small zeolitic fragments in the pore walls,^{3,4,6} (iv) ordered⁷ or disordered^{8,9} mesoporous materials with zeolitic walls, (v) zeolite nanocrystals dispersed into a mesoporous materials with either amorphous or zeolitic walls,¹⁰ (vi) nanocrystals^{11,12} and nanosheets of zeolite aggregates.¹³ Mesoporous zeolites with ordered MCM-41-like mesoporosity were prepared by micelle-templating of zeolites following different processes: (i) by a dissolution-reassembly process (e.g. ZSM-5,⁵ mordenite,³⁻⁶ beta¹⁴), (ii) by a surfactant-templating process without dissolution (e.g. FAU-Y⁷) and (iii) by a self-assembly process of nanozeolites precursor (e.g. beta¹⁵) or zeolite seeds (e.g. ZSM-5¹⁶).

The presence of bimodal porosity in mesoporous zeolites causes dramatic changes in many physicochemical properties compared to conventional zeolites. In catalysis, mesoporous zeolites typically exhibit enhanced accessibility for bulky molecules, which sizes exceed that of the micropores and a reduction of the diffusion path length. Generally, the enhanced intraparticle transport leads to higher catalytic activities, increases selectivity, and catalyst stability due to the reduction of secondary reactions and coking, respectively.¹⁷

Mesoporous zeolites present stronger acidity than purely mesoporous aluminosilicates such as Al-MCM-41, but often feature lower amount of Brønsted acid sites than pristine zeolites.^{5,7,10,18} However, judiciously selected treatment conditions in mesoporous zeolites synthesis permit to maintain their strong Brønsted acidity¹⁹ and micropore volumes.²⁰ Enhanced catalytic performances of mesoporous zeolites have often been proven. Numerous examples, such as the isopropylation of naphthalene²¹ and the liquid phase esterification of benzyl alcohol with hexanoic acid¹⁶ over mesoporous *BEA structured zeolite, the isomerization of 1,2,3-trimethylbenzene, the cracking of cumene²² or n-hexane,⁵ the methanol-to-hydrocarbon reaction² over mesoporous ZSM-5 are well documented. Similarly, mesoporous FAU-Y, MOR, *BEA, zeolite L (LTL) showed enhanced catalytic activity in the dealkylation of tri-isopropylbenzene compared to pristine zeolites.²³ Mesoporous mordenite prepared by micelle-templating showed remarkably high activity, stability, and selectivity toward the formation of diisopropylbiphenyls in the transalkylation of biphenyl with diisopropylbenzene.¹⁸ Mesoporous FAU-Y prepared by surfactant-templating allowed to

achieve higher gasoline yields in FCC and lower coke formation.^{24,25} In the hydrocracking of n-hexadecane, the comparison of mesoporous FAU-Y with a set of aluminated mesoporous silicas²⁶ showed that the catalytic activity relates linearly to the number of strong Brønsted acid sites, while selectivity, more precisely the yield in isomerization products, scaled directly with the mesopore volume of the catalyst. The number of strong Brønsted acid sites can be adjusted by tuning the synthesis conditions^{27,28} and appeared to be correlated to the micropore volume of the mesoporous zeolite.¹⁰

The influence of the micro-/ and mesopore surface areas in mesoporous zeolites in catalysis and adsorption is seldom discussed. In general only the total surface area calculated by the BET equation is given. This value, classically used to characterize zeolites textural properties, is far from being satisfactory and does not allow to elucidate the role of micro- and mesopore surface areas in the hierarchical materials. The *t*-plot analysis method allows theoretically such calculations and it was applied in few studies of mesoporous zeolites but mainly to determine external surface areas and micropore volumes.^{15,18,29,30} This method is however not straightforward. Indeed, computational studies proved that the *t*-plot method underestimates micropore volumes and overestimates mesopore surface areas of hierarchical micro-/mesoporous materials.³¹⁻³³ This was confirmed experimentally using mechanical mixtures of FAU-Y and MCM-41.^{34,35} Corrections of the *t*-plot method were provided to achieve calculations of micro- and mesopore volumes³⁴ and surface areas³⁵ for mesoporous FAU-Y.

These corrections were up to date limited to FAU structured zeolites. In the present study we present specific corrections of the *t*-plot for ZSM-5, *BEA and MOR structured zeolites, based on a set of mechanical mixtures of zeolites and MCM-41. The work is organized in three parts. In the first one, the surface area of the native zeolites (FAU, MFI, *BEA, MOR) determined by the BET method is discussed. This is of prime importance as the *t*-plot analysis uses BET area as total surface area for the calculations of micro- and mesopore surface areas for mesoporous zeolites. In the second part, corrections for *t*-plot analysis for each mesoporous zeolite were achieved using mechanical mixtures of native zeolites and MCM-41. In the third part, the corrected *t*-plot analysis was applied for the characterization of a great variety of mesoporous zeolites synthesized by micelle-templating.

EXPERIMENTAL SECTION

Mechanical mixtures of zeolites and Al-MCM-41. Al-MCM-41 was synthesized by mixing water, NaOH and octadecyltrimethylammonium bromide (C18TAB, from Aldrich) at 323 K to obtain a clear solution. Then silica powder (2.5 g) (Aerosil 200, Degussa) was added and the mixture was stirred for 20 min. The molar composition of the mixture was: 1 SiO₂: 0.1 C18TAB: 0.25 NaOH: 56 H₂O. The mixture was then transferred to an autoclave and placed in an oven at 388 K for 24 h. The recovered solid was filtrated, water washed until neutral pH, dried at 373 K for 24 h and calcined under air at 823 K for 8 h.

Commercial zeolites were purchased from Zeolyst: ZSM-5 with Si/Al = 15 (CBV 3024E, NH₄⁺ form, 10-MR, 3D, sinusoidal channels 5.1 x 5.5 Å, straight channels 5.3 x 5.6 Å, cavities in intersections 8-10 Å, FAU-Y with Si/Al = 15 (CBV 720, H⁺ form, 12MR, 3D, cavity 13 Å, window 7.4 Å), MOR with Si/Al = 10 (CBV21A, NH₄⁺ form, 12 and 8-MR, 2D,

straight channels 7.0 x 6.5 Å, side pockets 3.4 x 4.8 Å), *BEA with Si/Al = 12.5 (CP814E*, NH₄⁺ form, 12 MR, 3D, straight perpendicular channels 6.6 x 6.7 Å, short connections 5.6 x 5.6 Å (length 5 Å) between channels) (Figure S1).

Mechanical mixtures of commercial zeolites (ZSM-5, FAU-Y, MOR, *BEA) and Al-MCM-41 were prepared after drying the materials at 373 K and weight percentage were adjusted to obtain the following wt% in zeolites: 0, 10, 25, 50, 60, 70, 80, 90, 100 wt%.

Mesoporous zeolites synthesis. Mesoporous zeolites were synthesized by micelle-templating using the commercial zeolites purchased from Zeolyst (ZSM-5, FAU-Y, MOR, *BEA) in presence of C18TAB surfactant in basic media. The protocol used in the present study was adapted from Goto et al. (2002)⁵ for mesoporous ZSM-5 synthesis using less amount of surfactant and a simplified protocol. First, H₂O, NaOH and C18TAB were mixed at 323 K to obtain a clear solution. Then the zeolite powder (2.5 g) was added and the mixture was stirred for 20 min. The molar composition of the mixture calculated by assuming zeolites as pure silica (60 g/mol) is 1 SiO₂: 0.1 C18TAB: n NaOH: 56 H₂O with 0 < n < 1. Then the mixture was put in an autoclave at 383 K for 24 h, followed by a pH adjustment at pH 8.5 with HCl 2 M and a post-treatment step at 383 K for 24 h. After filtration and water washing until neutral pH, the samples were dried at 373 K for 24 h and calcined under air at 823 K for 8 h.

Characterization techniques.

N₂ sorption at 77 K. 100 mg of materials was used to get high precision in the mass determination of the samples and hence in the specific volumes and surface areas calculations. The samples were outgassed at 523 K for 24 h prior nitrogen sorption analysis at 77 K using a Micromeritics ASAP 2010 apparatus. Specific surface area was determined using the BET method. The relative pressure range to use the BET equation $(p/p_0)/[V(1-p/p_0) = f(p/p_0)]$ was determined thanks the superior limit given by the maximum of the Rouquerol curve $V(1-p/p_0) = f(p/p_0)$.³⁵⁻³⁷ Mesopore diameters were calculated by Broekhoff and De Boer (BdB) desorption method³⁸ at the inflexion point of the desorption step since it was demonstrated to be one of the most reliable methods for mesoporous materials such as MCM-41³⁹ based the good correspondence obtained with the mesopore diameters evaluated by geometrical calculations based on X-Ray diffraction (Figure S2). Values to transform the pressure into pore diameter have been presented in Table S1. Figure S2 shows that the BdB method leads to mesopore diameters similar to that obtained using the NLDFT method.⁴⁰ For *t*-plot analysis see the tutorial in Supp. Info. (Figures S3, S4, S5).

GCMC Simulations. Grand canonical Monte Carlo (GCMC) simulations were carried out at 77 K to predict the N₂ adsorption isotherm for BEA (polymorph B) using the Complex Adsorption and Diffusion Simulation Suite (CADSS) code. The isotherm was calculated for a pressure range from 10⁻⁶ to 1.0 bar. For each state point, 2×10⁷ Monte Carlo steps were used for both equilibration and production runs. The N₂/BEA interactions were treated by the sum of a coulombic term and a van der Waals contribution with the standard 12-6 Lennard-Jones (LJ) potential. The LJ parameters and charges for each zeolite framework atom were taken from June *et al.*⁴¹ while N₂ was described by a 3-LJ charged site model developed by Murthy *et al.*⁴² following the same strategy as reported by Snurr *et al.*⁴³. The corresponding LJ cross-parameters were obtained using the Lorentz–Berthelot combination.

The Ewald summation method was used to calculate the electrostatic interactions, and the treatment of the short-range interactions was considered with a cut off distance of 1.2 nm.

RESULTS AND DISCUSSION

Accuracy of BET equation for the determination of surface area of zeolites. The determination of the total surface area of mesoporous zeolites is needed to calculate micro- and mesopore surface area by t -plot analysis. Most experimental total surface areas are reported as BET areas (S_{BET}) derived from nitrogen isotherms at 77 K. Though the S_{BET} is well accepted to describe the total surface area for mesoporous materials, it is often stated that the use of the BET method is questionable for microporous materials.³⁷ Depending on the micropore size, the BET area can either undervalue, match, or overvalue the theoretical nitrogen-accessible surface area ($N_{2-a_{acc}}$) calculated from the crystal structure using a rigid spherical probe for nitrogen (0.373 nm diameter).^{43,44}

The BET calculation delivers an estimation of the nitrogen monolayer loading, which is then converted into a BET surface area. It was shown that nitrogen monolayers form in microporous graphene,⁴⁴ and that the choice of the pressure range for BET calculation is of prime importance. In order to estimate the correct pressure range, Rouquerol et al.,^{36,37} suggested four BET consistency criteria:

1. Only a pressure range where $V(1-p/p_0)$ increases monotonically with p/p_0 should be selected and the maximum value $(p/p_0)_{max}$ should be chosen as the highest limit of the pressure range for BET calculation.
2. The value of C_{BET} resulting from the linear regression should be positive.
3. The monolayer loading V_m resulting from the linear regression should correspond to a relative pressure $(p/p_0)_m$ falling within the selected linear region: $(p/p_0)_m \leq (p/p_0)_{max}$
4. The calculated relative pressure $(p/p_0)_{m-cal}$ corresponding to the theoretical monolayer loading issued from the BET equation (Eq. 1, 2) should be equal to $(p/p_0)_m$ with a tolerance of 20%. $(p/p_0)_{m-cal}$ is obtained by replacing V by V_m and (p/p_0) by $(p/p_0)_{m-cal}$ in the BET equation (Eq. 1):

$$\frac{p/p_0}{V(1-p/p_0)} = \frac{1}{V_m C_{BET}} + \frac{C_{BET} - 1}{V_m C_{BET}} (p/p_0) \quad (1)$$

with V_m corresponding to the monolayer volume and C_{BET} is a constant related to the energetics of adsorption of nitrogen with the surface, e.g. its affinity to the surface.

When $(p/p_0) = (p/p_0)_{m-cal}$ and $V = V_m$, Eq. 1 becomes Eq. 2:

$$\left(\frac{p}{p_0} \right)_{m-cal} = \frac{1}{1 + \sqrt{C_{BET}}} \quad (2)$$

The four criteria have to be satisfied to calculate precisely S_{BET} .

Snurr et al.^{43,44} compared theoretical nitrogen-accessible surface area ($N_2\text{-}a_{\text{acc}}$) with BET areas calculated from the GCMC simulated nitrogen adsorption isotherms at 77 K for different kind of microporous materials as graphenes, MOFs and zeolites. For model slit-pores materials as graphenes,^{44,45} BET areas fairly match with $N_2\text{-}a_{\text{acc}}$ for pore diameter ranging from 0.66 to 0.96 nm (equal to 1.8 to 2.6 times the size of the nitrogen molecule) corresponding to monolayer coverage and for pore diameter ≥ 1.47 nm, e.g. higher than 4 times the size of the nitrogen molecule. BET areas underestimate $N_2\text{-}a_{\text{acc}}$ for pore diameter from 0.37 to 0.63 nm equal to 1 – 1.7 times the size of the nitrogen molecule, as the hard sphere probe molecule has access to the whole surface of the pores, whereas soft nitrogen molecules during surface coverage are not all in contact with the surface due to steric hindrance. BET areas overestimate $N_2\text{-}a_{\text{acc}}$ in two cases: (i) for pores with diameter smaller than 0.36 nm as the hard sphere probe molecule cannot access the pores whereas “soft” nitrogen can, then in this case $N_2\text{-}a_{\text{acc}}$ underestimates the surface accessible to nitrogen, (ii) for pores with diameter from 1.0 to 1.33 nm equal to 2.7 – 3.6 times the size of nitrogen molecules due to “pore filling contamination”. Pore filling occurs simultaneously as monolayer coverage. Molecules that are not in direct contact with the pore walls are erroneously counted by the BET method as contributing to the monolayer. In this case, it appears that $(p/p_0)_{\text{m-cal}}$ should be used instead of $(p/p_0)_{\text{max}}$ in the BET calculation to limit the overestimation of S_{BET} by 16% in comparison to the theoretical $N_2\text{-}a_{\text{acc}}$ value, especially when a secondary sharp volume increase occurs in nitrogen adsorption isotherm in log scale.⁴⁴

The surface areas of more than 200 MOFs were examined.^{43,44,46,47} For 11 MOFs, BET calculations that fulfill all Rouquerol criteria were found to overestimate $N_2\text{-}a_{\text{acc}}$.⁴⁴ Lin et al.⁴⁶ compared the true monolayer surface area with the BET area and $N_2\text{-}a_{\text{acc}}$. They showed that for MOFs with true monolayer areas between 1500 and 3500 m^2/g , BET and $N_2\text{-}a_{\text{acc}}$ areas predict the true monolayer area fairly well, even though few outliers still exist (essentially due to pore filling contamination or the existence of multiporosity).⁴⁶ BET areas generally agree with the true monolayer areas if the surface areas are smaller than 1500 m^2/g , while $N_2\text{-}a_{\text{acc}}$ underestimates the true monolayer areas, due essentially to the presence of micropores with a pore diameter lower than 0.4 nm.⁴⁶ For MOFs with true monolayer areas larger than 3500 m^2/g , most of the structures have a combination of large micropores (1 - 2 nm) and small mesopores (2 - 3 nm) and BET method overestimates the surface areas, while $N_2\text{-}a_{\text{acc}}$ leads to comparable than the true monolayer areas.⁴⁶ S_{BET} overestimates true monolayer area if different sizes of micropores are present in the materials due to pore filling contamination of the smallest one.

In summary, the exploration of graphenes and MOFs leads to the following relationship between true monolayer area ($S_{\text{monolayer}}$), BET areas and $N_2\text{-}a_{\text{acc}}$ with different pore diameters (D):

$$\begin{array}{ll}
 D \leq 0.36 \text{ nm:} & S_{\text{BET}} = S_{\text{monolayer}} > N_2\text{-}a_{\text{acc}} \\
 0.37 < D < 0.63 \text{ nm:} & S_{\text{BET}} = S_{\text{monolayer}} < N_2\text{-}a_{\text{acc}} \text{ (not complete monolayer} \\
 & \text{formation)} \\
 0.66 < D < 0.96 \text{ nm slit-pores:} & S_{\text{BET}} = S_{\text{monolayer}} = N_2\text{-}a_{\text{acc}} \text{ (monolayer formation)}
 \end{array}$$

0.75 < D < 1.12 nm non-slit pores: $S_{\text{BET}} > S_{\text{monolayer}} = N_2\text{-}a_{\text{acc}}$ (monolayer formation, but overestimation by pore filling contamination).

1.00 < D < 1.33 nm slit-pores: $S_{\text{BET}} > S_{\text{monolayer}} = N_2\text{-}a_{\text{acc}}$ (pore filling contamination)

1.47 < D < 3.0 nm slit-pores: $S_{\text{BET}} = S_{\text{monolayer}} = N_2\text{-}a_{\text{acc}}$ (monolayer formation)

1.5 < D < 2.5 nm non-slit pores: $S_{\text{BET}} > S_{\text{monolayer}} = N_2\text{-}a_{\text{acc}}$ (pore filling contamination)

Snurr et al.⁴³ equally examined surface areas of zeolites. They demonstrated that 4 zeolites (MFI, BOG, LTA, FAU) featured BET areas matching with $N_2\text{-}a_{\text{acc}}$.⁴³ MOR featured an overestimation of BET area in comparison to $N_2\text{-}a_{\text{acc}}$ attributed to the presence of small side pockets (0.34 x 0.48 nm) in the crystals, which are less accessible to the hard spherical probes (0.373 nm diameter) used for $N_2\text{-}a_{\text{acc}}$. Without the consideration of the side pockets, BET area of MOR main channels (0.7 x 0.65 nm) matched well with $N_2\text{-}a_{\text{acc}}$.⁴³ Snurr et al.⁴⁴ recommended that the quality of crystalline microporous materials (MOFs, zeolites) should be assessed by comparing its experimental BET area to the BET area calculated from the GCMC simulated nitrogen adsorption isotherm for the crystal structure and not to the $N_2\text{-}a_{\text{acc}}$, making sure that the four BET Rouquerol criteria are applied to select the pressure range for the BET calculations. The BET areas for microporous materials are the apparent surface areas identified by nitrogen.

In the present study, experimental and GCMC simulated nitrogen isotherms were used to compare BET areas with their $N_2\text{-}a_{\text{acc}}$ (Figure 1) for the native zeolites ZSM-5 (MFI crystal structure), MOR, *BEA, FAU-Y. The Rouquerol criteria were verified (Table 1). $(p/p_0)_{\text{max}}$ were first determined (criterion 1) and the linear regression from this relative pressure allowed to determine the pressure domain for the BET calculation. The C_{BET} were calculated and were found positive (criterion 2). The monolayer volumes (V_m) were assessed and the corresponding relative pressures determined $(p/p_0)_m$. They were accurately comprised in the selected linear region of relative pressures (criterion 3). The predicted $(p/p_0)_{m\text{-cal}}$ calculated from the BET equation (Eq. 2) were in agreement with $(p/p_0)_m$ with a tolerance of $\pm 20\%$ (criterion 4), except for MOR. The present zeolites fulfilled the four Rouquerol criteria, except MOR, which fulfill 3 of them (not criteria 4th) (Table 1).

Table 1. Verification of the four Consistency Rouquerol Criteria for BET Areas (S_{BET}) Calculation for Zeolites

Criteria	1 st	3 rd	2 nd	3 rd	4 th		
Zeolites	$(p/p_0)_{\text{max}}$	(p/p_0) domain	C_{BET}	V_m cm ³ STP/g	S_{BET} m ² /g	$(p/p_0)_m$	$(p/p_0)_{m\text{-cal}}$
ZSM-5	0.060	0.008 - 0.060	3093	85	373	0.019	0.018
MOR	0.030	0.010 - 0.030	9713	121	527	0.015	0.010
FAU-Y	0.043	0.001 - 0.043	2304	217	946	0.023	0.020
*BEA	0.070	0.010 - 0.070	1313	139	606	0.030	0.027

The experimental S_{BET} were compared to $N_2\text{-}a_{\text{acc}}$ (Figure 1) calculated geometrically by applying a Monte Carlo (MC) integration technique as implemented in Zeo++⁴⁸ to the crystal

structures given by International Zeolite Association (IZA) using a model of hard spheres for nitrogen with a probe diameter equal to the van der Waals diameter of nitrogen ($2^{1/6}\sigma = 0.373$ nm) as recommended by previous theoretical studies.⁴³ Experimental S_{BET} were also compared to S_{BET} calculated from the GCMC simulated nitrogen isotherms⁴³ (Figure 1) in the pressure domain following the Rouquerol criteria. GCMC simulations revealed that a major fraction of nitrogen molecules lie flat on the micropore surface.⁴³

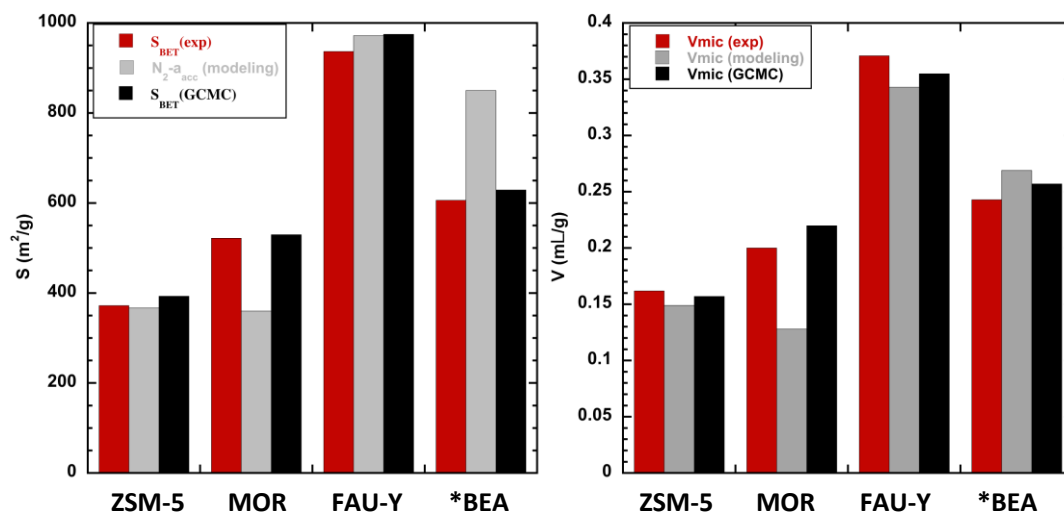


Figure 1. (left) S_{BET} determined from (red) experimental and (black) GCMC simulated nitrogen isotherms following the Rouquerol criteria; (grey) geometrical N_2 - a_{acc} for “hard” spherical N_2 probes of 0.373 nm diameter. Note: the GCMC simulated S_{BET} were taken from literature⁴³ for MFI, MOR FAU-Y while the data for *BEA polymorph B was obtained in this work using the same force field parameters and charges for both N_2 and zeolites as reported in ref. 43). (right) corresponding micropore volumes of native zeolites.

S_{BET} calculated from the experimental and simulated nitrogen isotherms (Figure 1) are in good agreement for the four zeolites. This emphasizes the good quality of the commercial zeolites and a good activation of all the samples prior to the experimental nitrogen isotherm measurements. BET areas agree with N_2 - a_{acc} for ZMS-5 and FAU-Y revealing that for these zeolites BET areas represent the true accessible surface areas of the crystal. This result was not expected since ZSM-5 features a micropore diameter around 0.55 nm for which BET area should underestimate N_2 - a_{acc} as explained above. On the other hand the presence of the intersections of 0.8 – 1.0 nm diameter in the MFI structure should overestimate N_2 - a_{acc} . It hence seems reasonable to assess that for ZSM-5 the overestimation of N_2 - a_{acc} resulting from the intersections compensates the underestimation of N_2 - a_{acc} in pore channels (Figure S6). For MOR, BET area overestimates N_2 - a_{acc} as previously reported⁴³ due to the presence of side pockets (0.34 nm x 0.48 nm) inaccessible to the model of hard spheres. For *BEA, BET areas underestimate N_2 - a_{acc} , which corresponds in fact to N_2 - a_{acc} overestimating the true monolayer, whatever the polymorph of *BEA is used. Here again, this deviation was not expected as

*BEA features channels of around 0.7 nm diameter for which BET area should be equal to N_2 - a_{acc} .⁴⁴ This difference might be related to the particular structure of *BEA. Indeed, the intersections of the perpendicular straight channels (0.76 nm x 0.64 nm) of *BEA along *a* and *b*, results in short channels (diameter 0.55 nm x 0.55 nm) along *c* with a length inferior to 0.5 nm. Two layers of nitrogen molecules cannot be found in these short connecting channels, whereas they are counted in the N_2 - a_{acc} using a rolling hard sphere probe leading to the overestimation of the nitrogen monolayer (Figure S7). The use of a larger hard spherical probe (0.5 nm), which cannot enter in the short intersections leads to an agreement between BET areas and N_2 - a_{acc} (637 m²/g). The micropore volumes obtained from experimental and simulated nitrogen adsorption compare well (Figure 1), as well as with the one determined by modeling with hard sphere, except for MOR, which showed a lower micropore volume by modeling due to the restricted accessibility of the hard spherical probe to the side pockets.

Textural features of commercial zeolites are given in Table 2. The *t*-plot analysis of the zeolites was performed to determine the external surface area (Figure S4). Home-made Al-MCM-41(C18) with mesopore diameter of 4.1 nm was added in Table 2 for comparison.

Table 2. Characterization of the commercial zeolites and home-made Al-MCM-41.

Materials	ZSM-5	BEA*	MOR	FAU-Y	Al-MCM-41
Si/Al	15	12.5	10	15	15
Particle size (nm)	50-150	30 ^a	100-500 ^a	500-1000	100 ^a
S_{BET} (m ² /g)	372	606	522 ^b	937	846
S_{ext} (m ² /g)	53	186	34	99	226
S_{mic} (m ² /g)	319	420	488	832	0
S_{mes} (m ² /g)	0	0	0	0	625
V_{mic} (mL/g)	0.162	0.243	0.210 ^b	0.371 ^c	0
V_{mes} (mL/g)	0	0	0	0	0

^aagglomeration of particles

^bwithout the side pockets (by simulation): $S_{BET} = 359$ m²/g, $V_{mic} = 0.128$ mL/g

^cwith a volume of the supercage of 0.28 mL/g

Zeolites and Al-MCM-41 were mixed in different mass ratio to calculate the real micro- and mesopore volumes and surface areas of the mixtures by linear combination and compared to the values obtained by *t*-plot analysis (Figure 2). Previously we revealed for hierarchical micro-/mesoporous materials featuring mesopore diameter equal or larger than 4 nm that N_2 - a_{acc} match the S_{BET} when the Rouquerol criteria were fulfilled.³² In the following, S_{BET} for mesoporous zeolites (or for the mixture of zeolites and Al-MCM-41) will be taken as total surface area and will be calculated following the Rouquerol criteria using a cross-sectional area of nitrogen molecules of 0.162 nm². The micropore (V_{mic}) and total (V_{tot}) pore volumes and the mesopore plus external surface areas ($S_{mes+ext}$) of mesoporous zeolites will be determined by *t*-plot analysis (see tutorial for *t*-plot analysis in Supplementary Information). The micropore surface area and the mesoporous volume will be determined by subtracting $S_{mes+ext}$ from the total surface area (S_{BET}) and V_{mic} from V_{tot} , respectively.

Corrections of t -plot analysis for mechanical mixtures of ZSM-5 and Al-MCM-41. By comparison with FAU-based zeolites,^{34,35} the family of ZSM-5 is more complex to characterize by N_2 adsorption isotherm at 77 K, as the shape of the isotherms is strongly impacted by the Si/Al ratio. In high silica ZSM-5 (Si/Al > 20), a sub-step at around $p/p_0 = 0.2$ is observed,⁴⁹ which origin is probably related to a structural transition of the zeolite framework from monoclinic to orthorhombic symmetry.⁵⁰ This sub-step is steep for MFI-type zeolite (ZSM-5 and Silicalite-1) with Si/Al > 60 and becomes smoother ($0.1 < p/p_0 < 0.3$) for Si/Al < 50. This sub-step renders the t -plot analysis more complex for MFI-type zeolite compared to other zeolites, for which the adsorption isotherm reaches a plateau at $p/p_0 < 0.1$, indicating the completion of micropore filling at this pressure. For ZSM-5 (Si/Al = 15), the t -plot analysis (Figure S4) shows that the total pore volume is reached at $t = 4.93$ Å, corresponding to a $p/p_0 = 0.32$ and to a micropore volume of 0.162 mL/g. The micropore volume (V_{mic})_{tpt} achieved by t -plot analysis in the fitting range $3.2 < t < 4.2$ Å amounts to 0.095 mL/g, clearly indicating the underestimation of micropore volume by this method, as previously demonstrated for FAU-Y.^{34,35}

Mechanical mixtures of ZSM-5 (Si/Al = 15) and Al-MCM-41 were prepared to evaluate the underestimation of the micropore volume and the overestimation of the mesopore surface area by t -plot analysis (Figure 2). A similar correction as for FAU-Y has been found for the micropore volume for mixtures with more than 20% micropore volume. A slightly larger correction is needed for mesopore plus external surface areas. The following corrections (Eq 3-5) were found, which allow to achieve the exact values of V_{mic} and $S_{mes+ext}$ for the mechanical mixtures of ZSM-5 and Al-MCM-41:

$$\text{for all } (V_{mic}/V_{tot})_{tpt} \quad S_{mes+ext}^* = (S_{mes+ext})_{tpt} [1 - (V_{mic}/V_{tot})_{tpt}] \quad (3)$$

$$0.04 < (V_{mic}/V_{tot})_{tpt} < 0.1 \quad V_{mic}^* = 2 (V_{mic})_{tpt} \quad (4)$$

$$(V_{mic}/V_{tot})_{tpt} > 0.15 \quad V_{mic}^* = 1.6 (V_{mic})_{tpt} \quad (5)$$

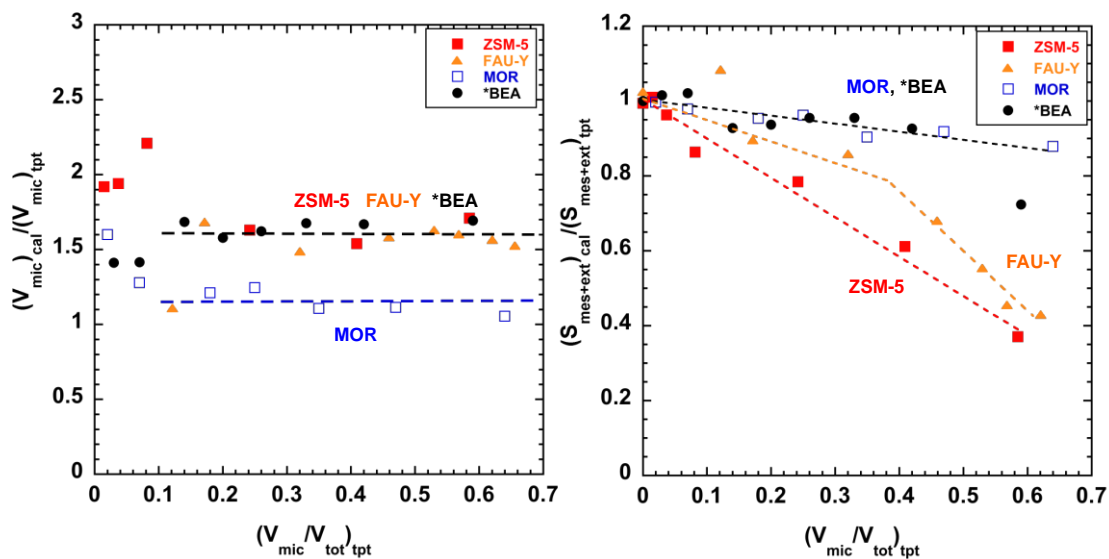


Figure 2. Comparison of t -plot determination of (left) V_{mic} and (right) $S_{\text{mes+ext}}$ with calculated values from the weight percentage of Al-MCM-41 and zeolites: (triangles) FAU-Y, (plain squares) ZSM-5, (empty squares) MOR, (circles) *BEA.

Corrections of t -plot analysis for mechanical mixtures of *BEA and Al-MCM-41. Mechanical mixtures of *BEA (Si/Al = 12.5) and Al-MCM-41 were prepared to evaluate the underestimation of the micropore volume and the overestimation of the mesopore surface area by t -plot analysis (Figure 2). A similar correction as for FAU-Y and ZSM-5 was found for the micropore volume for mixtures with more than 13% micropore volume. However a lower correction than for FAU-Y and ZSM-5 was needed for the mesopore plus external surface area, which was very close to the calculated value ($1 > (S_{\text{mes+ext}})_{\text{cal}} / (S_{\text{mes+ext}})_{\text{tpt}} > 0.9$). The following corrections (Eq 6-8) were found, which allow to achieve the exact values of V_{mic} and $S_{\text{mes+ext}}$ for the mechanical mixtures of *BEA and Al-MCM-41:

$$(V_{\text{mic}}/V_{\text{tot}})_{\text{tpt}} < 0.42 \quad S_{\text{mes+ext}}^* = (S_{\text{mes+ext}})_{\text{tpt}} [1 - 0.2 (V_{\text{mic}}/V_{\text{tot}})_{\text{tpt}}] \quad (6)$$

$$(V_{\text{mic}}/V_{\text{tot}})_{\text{tpt}} < 0.07 \quad V_{\text{mic}}^* = 1.4 (V_{\text{mic}})_{\text{tpt}} \quad (7)$$

$$(V_{\text{mic}}/V_{\text{tot}})_{\text{tpt}} > 0.13 \quad V_{\text{mic}}^* = 1.6 (V_{\text{mic}})_{\text{tpt}} \quad (8)$$

Corrections of t -plot analysis for mechanical mixtures of MOR and Al-MCM-41. Mechanical mixtures of MOR (Si/Al = 10) and Al-MCM-41 have been prepared to evaluate the underestimation of the micropore volume and the overestimation of the mesopore surface area by t -plot analysis (Figure 2). A lower correction than for FAU-Y, ZSM-5 and *BEA was found for the micropore volume for mixtures with more than 15% micropore volume. For MOR featuring a pseudo mono-dimensional micropore structure almost no correction of t -plot analysis was needed. $(V_{\text{mic}})_{\text{tpt}}$ was very close to the calculated micropore volume ($(V_{\text{mic}})_{\text{cal}} / (V_{\text{mic}})_{\text{tpt}} = 1.16$). Also, as for *BEA, low correction was needed for the mesopore plus external surface area, which was very close to the calculated value ($1 > (S_{\text{mes+ext}})_{\text{cal}} / (S_{\text{mes+ext}})_{\text{tpt}} > 0.9$). The following corrections (Eq 7-9) were found, which allowed to achieve the exact values of V_{mic} and $S_{\text{mes+ext}}$ for the mechanical mixtures of MOR and Al-MCM-41:

$$\text{for all } (V_{\text{mic}}/V_{\text{tot}})_{\text{tpt}} \quad S_{\text{mes+ext}}^* = (S_{\text{mes+ext}})_{\text{tpt}} [1 - 0.2 (V_{\text{mic}}/V_{\text{tot}})_{\text{tpt}}] \quad (7)$$

$$(V_{\text{mic}}/V_{\text{tot}})_{\text{tpt}} < 0.15 \quad V_{\text{mic}}^* = (V_{\text{mic}})_{\text{tpt}} [1.6 - 2.9 (V_{\text{mic}}/V_{\text{tot}})_{\text{tpt}}] \quad (8)$$

$$(V_{\text{mic}}/V_{\text{tot}})_{\text{tpt}} > 0.15 \quad V_{\text{mic}}^* = 1.16 (V_{\text{mic}})_{\text{tpt}} \quad (9)$$

Characterization of mesoporous zeolites prepared by micelle-templating. Families of mesoporous zeolites (FAU, MFI, MOR and *BEA) were synthesized by micelle-templating based on modifications and simplifications of the two steps procedure initially described by Goto *et al.*⁵ for ZSM-5 and MOR. The synthesis involves a hydrothermal

treatment in basic conditions with different amount of NaOH in the presence of a surfactant (C18TAB) followed by a pH adjustment prior to a second hydrothermal treatment (Figure 3). The one-step procedure previously described for mesoporous FAU-Y^{10,34,35} was not efficient for ZSM-5, therefore the two-steps procedure was applied to all the zeolites.

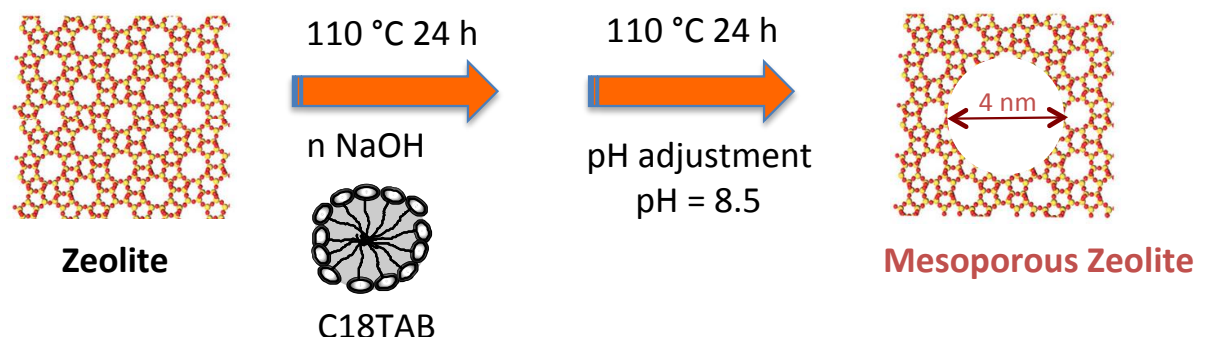


Figure 3. Schematic representation of the two-steps procedure for the synthesis of mesoporous zeolites by micelle-templating.

Goto *et al.*⁵ described the resulting materials as zeolite/mesoporous molecular sieve composites produced by a dissolution/reconstruction or reassembly process. The mechanism of mesoporous MOR formation was studied in detail by Ivanova *et al.*^{4,6} and different kinds of mesoporous zeolites were obtained depending on the degree of zeolite dissolution and the extent of mesoporous phase overgrowth: zeolite nanocrystals coated with mesoporous materials at low transformation levels and mesoporous materials containing zeolite fragments in the mesopore walls at high transformation levels.^{4,6} The stepwise hydrothermal treatment with the intermediate pH regulation was shown to enhance the condensation of siliceous species formed during desilication, to lead to their rearrangement into an ordered mesoporous phase, such as Al-MCM-41, and to result in the product yields of 100%.⁴ Unlike Al-MCM-41, these materials show a strong zeolites-like acidity and have proven to be useful for catalysis due to high acidity and improved textural properties.^{5,14,16,18,23-28} However the NaOH content used in the micelle-templating synthesis revealed to impact acidic properties and generally increasing alkalinity leads to a decrease in acidity in comparison to the native zeolite.^{4,10} A good compromise has to be found between the remaining strong zeolites-like acidity and the amount of additional mesopores created by micelle-templating. Micro- and mesopore surface areas and volumes have to be precisely analyzed to better characterize these families of mesoporous zeolites. The textural properties of the mesoporous zeolites were analyzed from their nitrogen isotherms (Figure 4) and *t*-plot curves (Figure S5) and the resulting values were modified using the corrected *t*-plot method provided above.

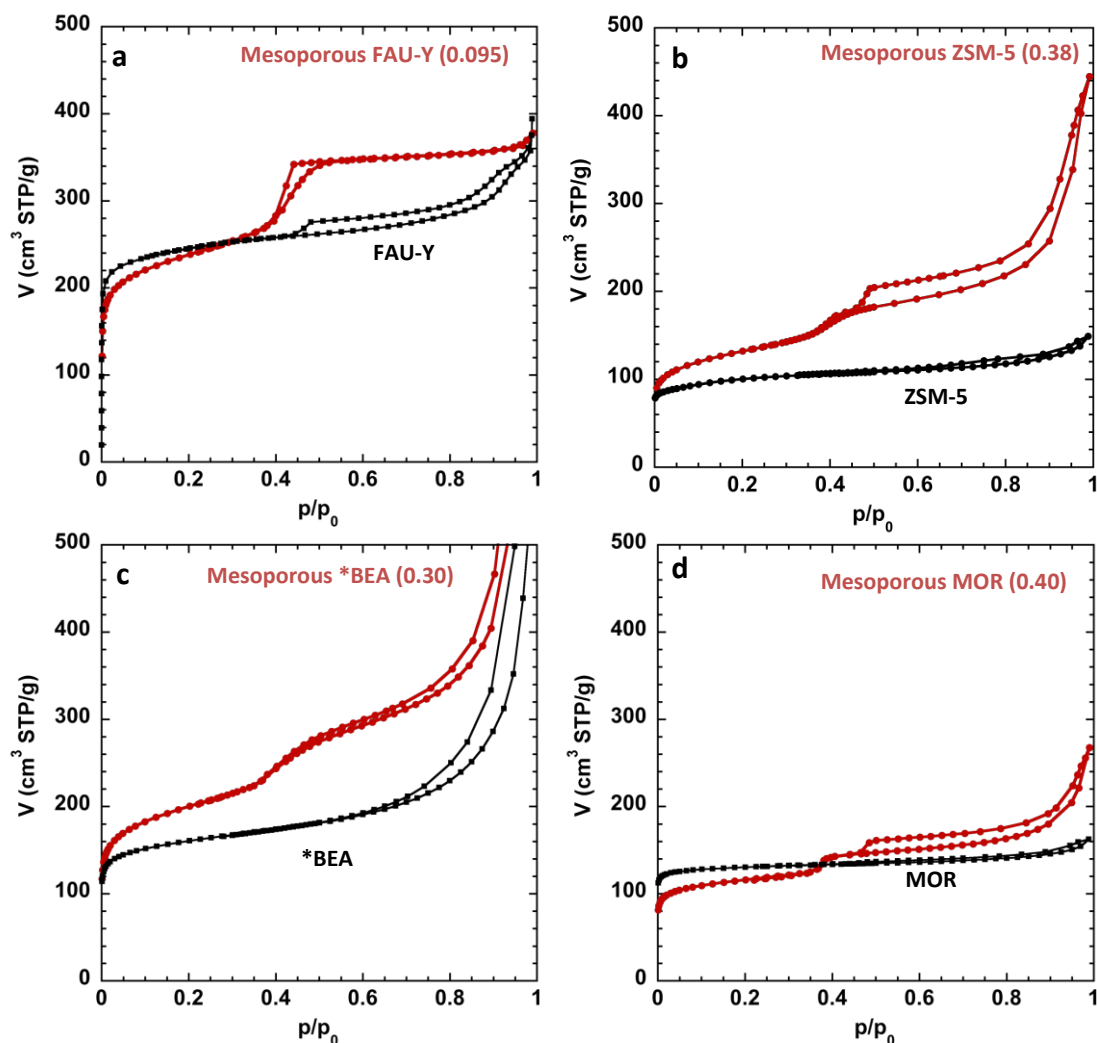


Figure 4. Nitrogen sorption isotherms at 77 K of the starting zeolites and of some examples of the mesoporous zeolites prepared by micelle-templating by the two steps procedure (in bracket is indicated the NaOH/Si ratio used in the synthesis).

Characterization of mesoporous FAU-Y. A new family of mesoporous FAU-Y was synthesized by the two steps procedure (instead of the previous one-step procedure)^{10,34,35} using a molar composition of: 1 SiO₂: 0.1 C18TAB: n NaOH: 50 H₂O with 0 < n < 0.15. XRD showed the presence of both FAU-Y zeolite framework and hexagonally ordered mesopores as in Al-MCM-41 (Figure S9). N₂ sorption isotherms at 77 K were recorded (Figures 4, S8). Mesopore diameters of the achieved family of mesoporous FAU-Y materials were around 4.3 nm (Table S3) in accordance with a micelle-templating mechanism with C18TAB surfactant as for Al-MCM-41.⁵¹ *t*-plot analyses were performed from the nitrogen adsorption isotherms. The *t*-plot corrections for FAU-Y (Figure 2) were applied (noted * in the following) to characterize the micro- and mesopore plus external surface areas and the micro- and mesopore volumes of mesoporous FAU-Y (Figure 5). By increasing the amount of

NaOH, the micropore volume and surface area decrease, while the mesopore volume and mesopore plus external surface area increase. The corrected t -plot analysis allows hence to select mesoporous FAU-Y with similar micro- and mesopore plus external surface areas or micro- and mesopore volumes with the aim to assess the impact of these parameters on catalytic reactions. For this family of mesoporous FAU-Y, the mesopore volume (V_{mes}^*) would be equivalent to the micropore volume (V_{mic}^*) (0.27 mL/g) for a synthesis performed with NaOH/Si = 0.087. The mesopore surface area plus external surface area ($S_{\text{mes+ext}}^*$) would be equivalent to the micropore surface area (S_{mic}^*) (450 m²/g) for a synthesis performed with NaOH/Si = 0.11 (Figure 5). These results differ very slightly (Figure S10) from the one obtained previously for mesoporous FAU-Y synthesized by the one-step procedure.^{10,34,35}

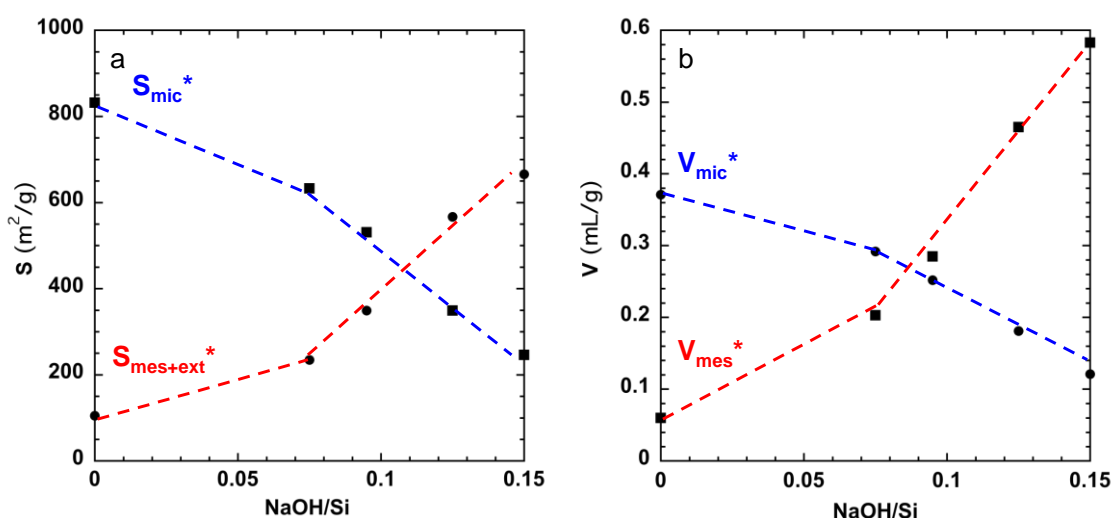


Figure 5. Micro- and mesopore (a) surface areas and (b) pore volumes calculated by corrected t -plot method determined for mechanical mixtures of Al-MCM-41 and FAU-Y (Si/Al = 15) of a family of mesoporous FAU-Y prepared from FAU-Y (Si/Al = 15) by micelle-templating using C18TAB and different amounts of NaOH by the two-steps procedure.

The external surface areas of the mesoporous FAU-Y are similar (around 60 m²/g) and the surface area developed only by the ordered mesopores can be calculated by subtraction (Table S3). It increases from 175 to 589 m²/g when NaOH/Si increases from 0.075 to 0.15.

Characterization of mesoporous ZSM-5. A family of mesoporous ZSM-5 was synthesized using the same protocol as for FAU-Y, but with a higher amount of NaOH corresponding to the molar composition: 1 SiO₂: 0.1 C18TAB: n NaOH: 56 H₂O with 0.3 < n < 0.7. XRD showed the presence of both ZSM-5 zeolite framework and hexagonally ordered mesopores as in Al-MCM-41 (Figure S11). N₂ sorption isotherms at 77 K were recorded (Figures 4, S8). Mesopore diameters of these hierarchical ZSM-5 were around 4.0 nm (Table S4) in accordance with a micelle-templating mechanism with C18TAB surfactant as for Al-MCM-41.⁵¹ The t -plot analyses were performed and corrections of t -plot values for ZSM-5

(Figure 2) were applied. The micro- and mesopore plus external surface areas and micro- and mesopore volumes of this mesoporous ZSM-5 family were calculated (Figure 6). The micropore surface area and volume were constant for mesoporous ZSM-5 synthesized with $0 < \text{NaOH/Si} < 0.30$, while the mesopore volume and the mesopore plus external surface area increased. For higher amounts of NaOH, the micropore volume and surface area decreased linearly with the increasing NaOH/Si ratio as the mesopore volume and the mesopore plus external surface area increased (Figure 6). It is hence possible to produce a mesoporous ZSM-5 with similar micropore volume ($V_{\text{mic}}^* = 0.15 \text{ mL/g}$) and surface area ($S_{\text{mic}}^* = 300 \text{ m}^2/\text{g}$) as the parent ZSM-5, but with additional mesoporosity ($V_{\text{mes}}^* = 0.10 \text{ mL/g}$, $S_{\text{mes+ext}}^* = 140 \text{ m}^2/\text{g}$) for a synthesis performed with NaOH/Si = 0.30. It is also possible to produce a mesoporous ZSM-5 with similar micro- and mesopore volume (0.14 mL/g) for a synthesis performed with NaOH/Si = 0.38 and equivalent micro- and mesopore surface area plus external surface area (250 m²/g) for a synthesis performed with NaOH/Si = 0.48.

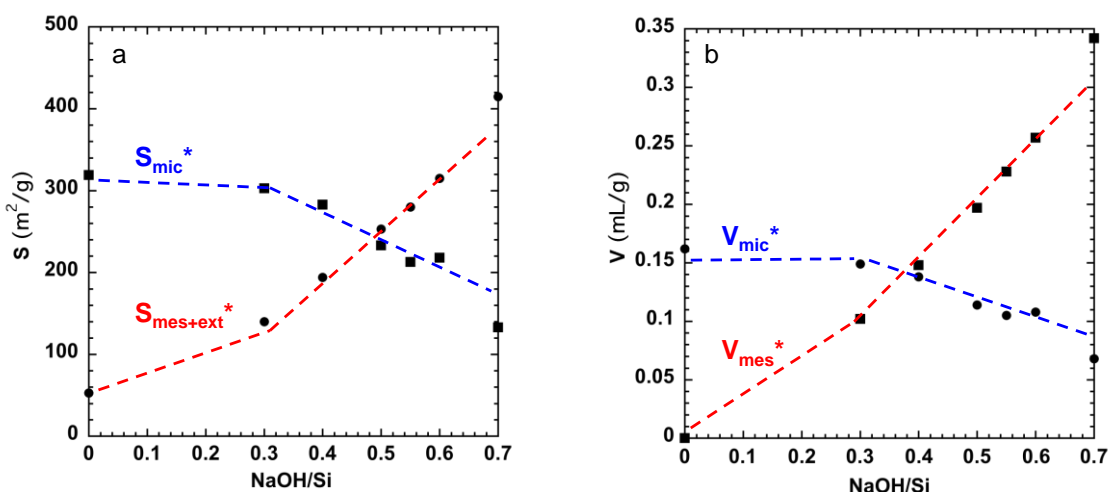


Figure 6. (a) Surface areas and (b) pore volumes calculated by corrected t -plot method determined for mechanical mixtures of Al-MCM-41 and ZSM-5 (Si/Al = 15) of a family of hierarchical ZSM-5 prepared from ZSM-5 (Si/Al = 15) by micelle-templating using C18TAB and different amounts of NaOH the two-steps procedure.

The external surface area (S_{ext}) of mesoporous ZSM-5 cannot be accurately calculated from the second part of the t -plot (Figure S5) as during the synthesis a secondary large porosity arises connected to the exterior of the crystals through the ordered mesopores evidenced in the nitrogen isotherm (Figure 4) by the step at high relative pressure and by the horizontal hysteresis leading to cavitation phenomena. The filling of such pores will take place simultaneously as the coverage of the external surface by nitrogen molecules leading to an overestimation of the external surface area (Table S4). This overestimation of S_{ext} will give an underestimation of the mesopore surface area. Only S_{mic}^* and $S_{\text{mes+ext}}^*$ calculated from the first part of the t -plot can be considered accurately.

Characterization of mesoporous MOR. A family of mesoporous MOR was synthesized from MOR (Si/Al = 10) by micelle-templating using the same protocol as FAU-Y and ZSM-5, with a similar NaOH/Si ratio as ZSM-5. The corresponding molar composition was: 1 SiO₂: 0.1 C18TAB: n NaOH: 56 H₂O with 0.2 < n < 0.8. XRD showed the presence of both MOR zeolite framework and hexagonally ordered mesopores as in Al-MCM-41 (Figure S12). N₂ sorption isotherms at 77 K were recorded (Figures 4, S8). The mesopore diameters of these mesoporous MOR were around 3.9 nm (Table S5) in accordance with a micelle-templating mechanism with C18TAB surfactant as for Al-MCM-41.⁵¹ The corrected *t*-plot method for MOR was applied (Figure 2) to assess micro- and mesopore volumes and micro- and mesoporous plus external surface areas (Figure 7). By increasing the NaOH ratio in the synthesis, the micropore volume and surface area decreased linearly with the increasing NaOH/Si ratio, while the mesopore volume and the mesopore plus external surface area increased (Figure 7). It is hence possible to produce a mesoporous MOR with equivalent micro- and mesopore volumes (0.11 mL/g) for a synthesis performed with NaOH/Si = 0.45, or with equivalent micro- and mesopore plus external surface area (220 m²/g) for a synthesis performed with NaOH/Si = 0.65.

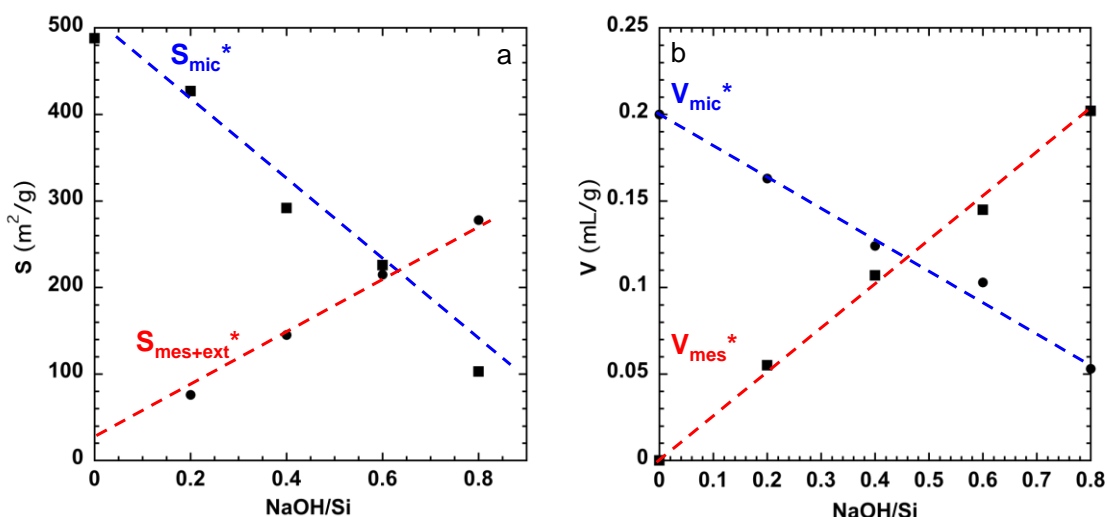


Figure 7. (a) Surface areas and (b) pore volumes calculated by corrected *t*-plot method determined for mechanical mixtures of Al-MCM-41 and MOR (Si/Al = 10) of a family of hierarchical MOR prepared from MOR (Si/Al = 10) by micelle-templating using C18TAB and different amounts of NaOH by the two steps procedure.

As for mesoporous ZSM-5, the external surface area (S_{ext}) of mesoporous MOR cannot be accurately calculated from the second part of the *t*-plot as during the synthesis also a secondary large porosity arises (Figure 4) leading to cavitation phenomena. The overestimation of S_{ext} (Table S5) will give an underestimation of the mesopore surface area. Only S_{mic}^* and $S_{mes+ext}^*$ calculated from the first part of the *t*-plot can be considered accurately.

Characterization of mesoporous *BEA. A family of mesoporous *BEA was synthesized from commercial *BEA (Si/Al = 12.5) by micelle-templating using the same protocol as for FAU-Y, ZSM-5 and MOR, with similar NaOH/Si ratios as ZSM-5 and MOR. The corresponding molar composition was: 1 SiO₂: 0.1 C18TAB: n NaOH: 56 H₂O with 0.1 < n < 0.6. XRD showed the presence of both *BEA zeolite framework and hexagonally ordered mesopores as in Al-MCM-41 (Figure S13). N₂ sorption isotherms at 77 K were recorded (Figures 4, S8). The mesopore diameter of these hierarchical *BEA were centered at 4.2 nm (Table S6) in accordance with a micelle-templating mechanism with C18TAB surfactant as for Al-MCM-41.⁵¹ The corrected *t*-plot analysis for *BEA (Figure 2) was applied to characterize the micro- and mesopore volumes and micropore and mesopore plus external surface areas of the family of mesoporous *BEA (Figure 8). The micropore volume remains constant close to the one of the parent zeolite (0.23 mL/g) for synthesis performed with NaOH/Si < 0.30, while the mesopore volume increases to reach 0.22 mL/g for the synthesis performed with NaOH/Si = 0.30 (Figure 8). This mesoporous *BEA should be potentially of high interest in catalytic processes. This material features a high micropore surface area (330 m²/g) and mesopore plus external surface area (400 m²/g). Unlike the micropore volume, the micropore surface area decreased linearly with the increase of NaOH/Si ratio, while the mesopore plus external surface area increased (Figure 8). A similar micropore surface area and mesopore plus external surface area (350 m²/g) is reached for a synthesis performed with NaOH/Si = 0.20.

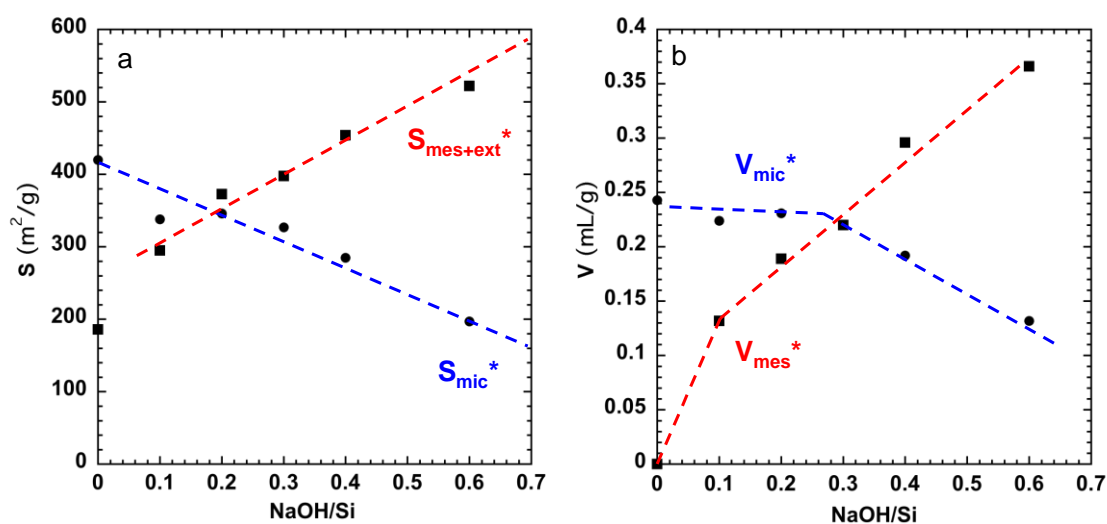


Figure 8. (a) Surface areas and (c) pore volumes calculated by corrected *t*-plot method determined for mechanical mixtures of Al-MCM-41 and *BEA (Si/Al =12.5) of a family of hierarchical *BEA prepared from *BEA (Si/Al = 12.5) by micelle-templating using C18TAB and different amounts of NaOH by the two steps procedure.

As for mesoporous ZSM-5 and MOR, the external surface area (S_{ext}) of mesoporous MOR cannot be accurately calculated from the second part of the *t*-plot as during the synthesis also a secondary large porosity arises leading to horizontal hysteresis (Figure 4), except for the

mesoporous *BEA synthesized with $\text{NaOH/Si} = 0.1$ (Figure S8). In this case S_{ext} is equal to $150 \text{ m}^2/\text{g}$ and the resulting mesoporous surface area is $146 \text{ m}^2/\text{g}$. For the mesoporous *BEA synthesized with higher amount of NaOH the overestimation of S_{ext} (Table S6) will give an underestimation of the mesopore surface area. Only S_{mic} and $S_{\text{mes+ext}}$ calculated from the first part of the t -plot can be considered accurately.

The corrected t -plot analysis presented in this study allowed to select mesoporous zeolites for example with either equal micropore and mesopore volumes or equal micropore and mesopore plus external surface area (Figure 9).

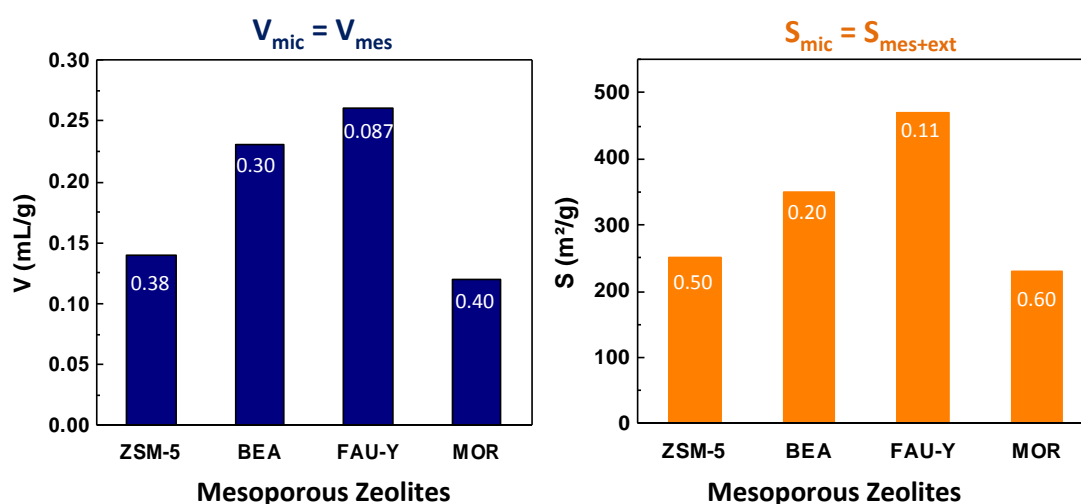


Figure 9. Pore volumes and surface areas of selected mesoporous zeolites prepared by micelle-templating (two-steps procedure) featuring either equal (left) micro- and mesopore volumes or (right) equal micropore and mesopore plus external surface areas. The NaOH/Si ratio used in the synthesis these mesoporous zeolites are indicated in each bars.

CONCLUSIONS

The classical t -plot method is known to underestimate micropore volume and overestimate mesopore surface area for hierarchical zeolites. Corrections initially provided for mesoporous FAU-Y were extended to other zeolites such as MFI, MOR and *BEA-type zeolites by the preparation of mechanical mixtures of Al-MCM-41 with these zeolites. Almost no corrections of t -plot analysis were found to be necessary for hierarchical MOR featuring a pseudo mono-dimensional micropore structure. The corrections of micropore volumes were similar for three-dimensional micropore structured zeolites (MFI, *BEA and FAU-Y), whereas new corrections were provided for the mesopore plus external surface areas for MFI and *BEA-type zeolites.

As t -plot method uses the total surface area S_{BET} in the calculation and as BET area for zeolites or more generally for microporous materials is a question of debate, we demonstrated that BET area matches the theoretical N_2 accessible surface area for FAU-Y. It is further the case for ZSM-5, but with a perfect compensation of the underestimation of the surface area of

the channels by the overestimation of the surface area of the intersections. For *BEA, the BET area represents the surface of the channels without the surface of the small connecting channels. For MOR, the BET area represents the surface of the channels plus the surface of the side pockets.

A set of mesoporous zeolites based on FAU-Y, ZSM-5, MOR, *BEA structures were further prepared by micelle-templating by a two-steps procedure. Their micro- and mesopore plus external surface areas and micro- and mesopore volumes were calculated by the new corrected *t*-plot methods. The presented methodology hence permits to produce mesoporous zeolites with adjustable textural properties: e.g. equivalent micropore volume or surface area as parent zeolites with an additional mesoporosity, or equivalent micro- and mesopore volumes, or equivalent micro- and mesopore plus external surface areas. These characterizations will be important to assess in the future how these parameters impact the catalytic activity of these porous materials.

ASSOCIATED CONTENT

Supporting information

Methodology for corrected *t*-plot method, *t*-plot curves of MCM-41, ZSM-5, mesoporous ZSM-5, comparison of BdB and NLDFT methods for mesopore diameter determination, data for BdB method, data for *t*-plot analysis with LiChrospher 1000, XRD of mesoporous zeolites, nitrogen isotherms of mesoporous zeolites.

AUTHOR INFORMATION

Corresponding Author

*E-mail: anne.galarneau@enscm.fr

ORCID

Anne Galarneau: [0000-0002-2076-058X](https://orcid.org/0000-0002-2076-058X)

Alexander Sachse: [0000-0001-5273-1313](https://orcid.org/0000-0001-5273-1313)

T. Jean Daou: [0000-0002-9973-3372](https://orcid.org/0000-0002-9973-3372)

Carla Vieira Soares: [0000-0003-0850-4230](https://orcid.org/0000-0003-0850-4230)

Guillaume Maurin: [0000-0002-2096-0450](https://orcid.org/0000-0002-2096-0450)

Notes

The authors declare no competing financial interest.

ACKNOWLEDGMENTS

AG thanks Pr Yasumoto Goto and Pr Randall Snurr for fruitful discussions on zeolite/mesoporous molecular sieve composites and on surface areas determinations of microporous materials by simulation.

REFERENCES

1. Tanabea, K.; Hölderich, W. F., Industrial application of solid acid-base catalyts. *Appl. Catal. A; Gen.* **1999**, *181*, 399-434.
2. Prech, J.; Pizzaro, P.; Serrano, D.P.; Cejka, J. From 3D to 2D zeolite catalytic materials. *Chem. Soc. Rev.* **2018**, *47*, 8263-8306.
3. Ivanova, I.I.; Knyazeva, E. E. Micro-mesoporous materials obtained by zeolite recrystallization: synthesis, characterization and catalytic applications. *Chem. Soc. Rev.* **2013**, *42*, 3671-3688.
4. Kasyanov, I.A.; Maerle, A.A.; Ivanova, I.I.; Zaikovskii, V.I. Towards understanding of the mechanism of stepwise zeolite recrystallization into micro/mesoporous materials. *J. Mater. Chem. A* **2014**, *2*, 16978-16988.
5. Goto, Y.; Fukushima, Y.; Ratu, P.; Imada, Y.; Kubota, Y.; Sugi, Y.; Ogura, M.; Matsukata M. Mesoporous material from zeolite. *J. Porous Mater.* **2002**, *9*, 43-48.
6. Ivanova, I.I.; Kasyanov, I.A.; Maerle, A.A.; Zaikovskii V.I. Mechanistic study of zeolites recrystallization into miro-mesoporous materials. *Microporous Mesoporous Mater.* **2014**, *189*, 163-172.
7. Sachse, A.; Grau-Atienza, A.; Jardim, E.O.; Linares, N.; Thommes, M.; Garcia-Martinez J. Development of intracrystalline mesoporosity through surfactant-templating. *Cryst. Growth Des.* **2017**, *17*, 4289-4305.
8. Na, K.; Jo, C.; Kim, J.; Cho, K.; Jung, J.; Seo, Y.; Messinger, R.J.; Chmelka, B.F.; Ryoo, R. Directing zeolites structures into hierarchically nanoporous architectures. *Science* **2011**, *333*, 328-332.
9. El Hanache, L.; Lebeau, B.; Nouali, H.; Toufaily, J.; Hamieh, T.; Daou, T. J. Performance of surfactant-modified *BEA-type zeolite nanosponges for the removal of nitrate in contaminated water: effect of the external surface. *J. Hazardous Mater.* **2019**, *364*, 206-217.
10. Mehlhorn, D.; Rodriguez, J.; Cacciaguera, T.; Andrei, R-D.; Cammarano, C.; Guenneau, F.; Gedeon, A.; Coasne, B.; Thommes, M.; Minoux, D.; Aquino, C.; Dath, J-P.; Fajula, F.; Galarneau A. Revelation on the complex nature of mesoporous FAU-Y zeolites. *Langmuir* **2018**, *34*, 11414-11423.
11. El Hanache, L.; Sundermann, L.; Lebeau, B.; Toufaily, J.; Hamieh, T.; Daou, T.J. Surfactant-modified MFI-type nanozeolites: super-adsorbents for nitrate removal from contaminated water. *Microporous Mesoporous Mater.* **2019**, *283*, 1-13.

12. Huve, J.; Daou, T.J.; Nouali, H.; Patarin, J.; Ryzhikov, A. The effect of nanostructures on high pressure intrusion-extrusion of water and electrolyte solutions in hierarchical nanoboxes of silicalite-1. *New J. Chem.* **2020**, *44*, 273-281.
13. Choi, M.; Na, K.; Kim, J.; Sakamoto, Y.; Terasaki, O.; Ryoo, R. Stable single-unit-cell nanosheets of zeolite MFI as active and long-lived catalysts. *Nature* **2009**, *461*, 246-249.
14. Suarez, N.; Perez-Pariente, J.; Mondragon, F.; Moreno, A. Generation of hierarchical porosity in beta zeolite by post-synthesis treatment with cetyltrimethylammonium cationic surfactant under alkaline conditions. *Microporous Mesoporous Mater.* **2019**, *280*, 144-150.
15. Al-Eid, M.; Ding, L.; Saleem, Q.; Badairy, H.; Sitepu, H.; Al-Maki, A. A facile method to synthesize hierarchical nano-sized zeolite beta. *Microporous Mesoporous Mater.* **2019**, *279*, 99-106.
16. Mukti, R.R.; Kamimura, Y.; Chaikittisilp, W.; Hirahara, H.; Shimojima, A.; Ogura, M.; Cheralathan, K.K.; Elangovan, S.P.; Itabashi, K.; Okubo, T. Hierarchically porous ZSM-5 synthesized by nonionic- and cationic-templating routes and their catalytic activity in liquid-phase esterification. *ITB J. Sci.* **2011**, *43A*, 59-72.
17. Hartmann, M.; Machoke, A. G.; Schweiger, W. Catalytic test reactions for the evaluation of hierarchical zeolites, *Chem. Soc. Rev.* **2016**, *45*, 3313-3330.
18. Ivanova, I.I.; Kuznetsov, A.S.; Yuschenko, V.V.; Knyazeva, E.E. Design of composite micro/mesoporous molecular sieve catalysts. *Pure Appl. Chem.*, **2004**, *76*, 1647-1658.
19. Gackowski, M.; Datka, J. Acid properties of hierarchical zeolites Y. *Molecules* **2020**, *25*, 1044-1068.
20. Chawla, A.; Linares, N.; Rimer, J.D.; Garcia-Martinez, J. Time-resolved dynamics of intracrystalline mesoporosity generation in USY zeolite. *Chem. Mater.*, **2019**, *31*, 5005-5013.
21. Choi, M.; Na, K.; Ryoo, R. The synthesis of a hierarchically porous BEA zeolite via pseudomorphic crystallization. *Chem. Comm.* **2009**, 2845-2847.
22. Srivasta, R.; Choi, M.; Ryoo, R. Mesoporous materials with zeolite framework: remarkable effect of the hierarchical structure for retardation of catalyst deactivation. *Chem. Comm.* **2006**, 4489-4491.
23. Al-Ani, A.; Haslam, J.J.C.; Mordvinova, N.E.; Lebedev, O.I.; Vicente, A.; Fernandez, C.; Zholobenko, V. Synthesis of nanostructured catalysts by surfactant-templating of large-pore zeolites. *Nanoscale Adv.* **2019**, *1*, 2029-2039.

24. Li, K.; Valla, J.; Garcia-Martinez, J. Realizing the commercial potential of hierarchical zeolites: new opportunities in catalytic cracking. *Chem. Cat. Chem.* **2014**, *6*, 46-66.
25. Garcia-Martinez, J.; Xiao, C.; Cychosz, K.A.; Li, K.; Wan, W.; Zou, X.; Thommes, M. Evidence of intracrystalline mesostructured porosity in zeolites by advanced gas sorption, electron tomography and rotation electron diffraction. *Chem. Cat. Chem.* **2014**, *6*, 3110-3115.
26. Vaugon, L.; Finiels, A.; Cacciaguera, T.; Hulea, V.; Galarneau, A.; Aquino, C.; Dath, J-P.; Minoux, D.; Gerardin, C.; Fajula, F. Impact of pore architecture on the hydroconversion of long chain alkanes over micro and mesoporous catalysts. *Petroleum Chem.* **2020**, *60*, 479-489.
27. Kazakov, M.O.; Nadeina, K.A.; Danilova, I.G.; Dik, P.P.; Klimov, O.V.; Pereyma, V.Y.; Gerasimov, E. Y.; Dobryakova, I.V.; Knyazeva, E.E.; Ivanova, I.I.; Noskov, A.S. Hydrocracking of vacuum gas oil over NiMo/ γ -Al₂O₃: effect of mesoporosity introduced by zeolite Y recrystallization. *Catal. Today* **2018**, *305*, 117-125.
28. Kazakov, M.O.; Nadeina, K.A.; Danilova, I.G.; Dik, P.P.; Klimov, O.V.; Pereyma, V.Yu.; Paukshtis, E.A.; Golubev, I.S.; Prosvirin, I.P.; Gerasimov, E.Yu.; Dobryakova, I.V.; Knyazeva, E.E.; Ivanova, I.I.; Noskov, A.S. Influence of USY zeolite recrystallization on physicochemical properties and catalytic performance of NiMo/USY-Al₂O₃ hydrocracking catalysts. *Catal. Today* **2019**, *329*, 108-115.
29. Suarez, N.; Perez-Pariente, J.; Mondragon, F.; Moreno, A. Generation of hierarchical porosity in beta zeolite by post-synthesis treatment with the cetyltrimethylammonium cationic surfactant under alkaline conditions, *Microporous Mesoporous Mater.* **2019**, *280*, 144-150.
30. Buttersack, C.; Mollmer, J.; Hofmann, J.; Glaser, R. Determination of micropore volume and external surface of zeolites, *Microporous Mesoporous Mater.* **2016**, *236*, 63-70.
31. Villemot, F.; Galarneau, A.; Coasne, B. Adsorption-based characterization of hierarchical metal-organic frameworks, *Adsorption* **2014**, *20*, 349-357.
32. Villemot, F.; Galarneau, A.; Coasne, B. Adsorption and dynamics in Hierarchical Metal Organic Frameworks, *J. Phys. Chem. C* **2014**, *118*, 7423-7433.
33. Coasne, B.; Galarneau, A.; Gerardin, C.; Fajula, F.; Villemot, F. Molecular Simulation of Adsorption and Transport in Hierarchical Porous Materials, *Langmuir* **2013**, *29*, 7864-7875.
34. Galarneau, A.; Villemot, F.; Rodriguez, J.; Fajula, F.; Coasne, B. Validity of the t-plot method to assess microporosity in hierarchical micro/mesoporous materials, *Langmuir* **2014**, *30*, 13266-13274.

35. Galarneau, A.; Mehlhorn, D.; Guenneau, F.; Coasne, B.; Villemot, F.; Minoux, D.; Aquino, C.; Dath, J-P. Specific surface area determination for microporous/mesoporous materials: the case of mesoporous FAU-Y, *Langmuir* **2018**, *34*, 14134-14142.
36. Rouquerol, F.; Rouquerol, J.; Imelik, B. Validité de la loi BET dans le cas de l'adsorption d'azote, d'argon et de butane sur des adsorbants poreux. *Bull. Soc. Chim. France*, **1964**, 635-639.
37. Rouquerol, J.; Llewellyn, P.; Rouquerol, F. Is the BET equation applicable to microporous adsorbents? *Stud. Surf. Sci. Catal.* **2007**, *160*, 49-56.
38. Broekhoff, J.C.P.; de Boer, J.H. Studies on pore systems in catalysts: XIII. Pore distributions from the desorption branch of a nitrogen sorption isotherm in the case of cylindrical pores B. Applications. *J. Catal.* **1968**, *10*, 377-390.
39. Galarneau, A.; Desplandier, D.; Dutartre, R.; Di Renzo, F. Micelle-templated silicates as a test bed for methods of mesopore size evaluation, *Microporous Mesoporous Mater.* **1999**, *27*, 297-308.
40. Neimark, A.V.; Ravikovitch, P.I. Capillary condensation in MMS and pore structure characterization. *Microporous Mesoporous Mater.* **2001**, *44-45*, 697-707.
41. Larry, J. R.; Bell, A. T.; Theodorou, D. N. Molecular dynamics study of methane and xenon in silicalite, *J. Phys. Chem.*, **1990**, *21*, 8232-8240.
42. Murthy, C. S.; Singer, K.; Klein, M. L.; McDonald, I. R. Pairwise additive effective potentials for nitrogen. *Molecular Physics*, **1980**, *41*, 1387-1399.
43. Bae, Y-S.; Yazaydin, A. O.; Snurr, R. Q. Evaluation of the BET method for determining surface areas of MOFs and zeolites that contain ultra-micropores, *Langmuir*, **2010**, *26*, 5475-5483.
44. Gomez-Gualdron, D.A.; Moghadam, P.Z.; Hupp, J.T.; Farha, O.M.; Snurr, R.Q. On the application of consistency criteria to calculate BET areas of micro- and mesoporous metal-organic frameworks, *J. Am. Chem. Soc.*, **2016**, *138*, 215-224.
45. De Lange, M.F.; Lin, L-C; Gascon, J.; Vlugt, T.J.H.; Kapteijn, F. assessing the surface area of porous solids: limitations, probe molecules, and methods. *Langmuir*, **2016**, *32*, 12664-12675.
46. Sinha, P.; Datar, A.; Jeong, C.; Deng, X.; Chung, Y.G.; Lin, L-C. Surface area determination of porous materials using the Brunauer-Emmett-Teller (BET) method: limitations and improvements. *J. Phys. Chem. C*, **2019**, *123*, 20195-20209.

47. Ambroz, F.; Macdonald, T.J.; Martis, V., Parkin, I.P. Evaluation of the BET theory for the characterization of meso and microporous MOFs. *Small Methods*, **2018**, *2*, 1800173 (1-17)
- 48- Willems, T.F.; Rycroft, C.H.; Kazi, M.; Meza, J.C.; Haranczyk, M. Algorithms and tools for high-throughput geometry-based analysis of crystalline porous materials. *Microporous Mesoporous Mater.* **2012**, *149*, 134-141.
49. Llewellyn, P.L.; Coulomb, J.P.; Grillet, Y.; Patarin, J.; Andre, G.; Rouquerol, J. Adsorption by MFI-type zeolites examined by isothermal microcalorimetry and neutron diffraction. 2. Nitrogen and carbon monoxide. *Langmuir* **1993**, *9*, 1852-1856.
50. Cho, H. S.; Miyasaka, K.; Kim, H.; Kubota, Y.; Takata, M.; Kitagawa, S.; Ryoo, R.; Terasaki, O. Study of argon gas adsorption in ordered mesoporous MFI zeolite framework. *J. Phys. Chem. C* **2012**, *116*, 25300-25308.
51. Di Renzo, F.; Galarneau, A.; Desplandier-Giscard, D.; Mastrantuono, L.; Testa, F.; Fajula, F. Formulation of Silica at the Nanometer Scale. *Chimica e l'Industria* **1999**, *81*, 587-591.

Graphical Abstract

